ASC Report No. 15/2016

Spurious modes of the complex scaled Helmholtz Equation

L. Nannen, M. Wess

Institute for Analysis and Scientific Computing —
Vienna University of Technology — TU Wien
www.asc.tuwien.ac.at ISBN 978-3-902627-05-6

Most recent ASC Reports

14/2016 *A. Bespalov, A. Haberl, and D. Praetorius*
Adaptive FEM with coarse initial mesh guarantees optimal convergence rates for compactly perturbed elliptic problems

13/2016 *J.M. Melenk and A. Rieder*
Runge-Kutta convolution quadrature and FEM-BEM coupling for the time dependent linear Schrödinger equation

12/2016 *A. Arnold and C. Negulescu*
Stationary Schrödinger equation in the semi-classical limit: Numerical coupling of oscillatory and evanescent regions

11/2016 *P.M. Lima, M.L. Morgado, M. Schöbinger and E.B. Weinmüller*
A Novel Approach to Singular Free Boundary Problems in Ordinary Differential Equations

10/2016 *M. Hanke, R. März, C. Tischendorf, E. Weinmüller, S. Wurm*
Least-Squares Collocation for Higher Index Differential-Algebraic Equations

9/2016 *A. Jüngel, P. Shpartko, and N. Zamponi*
Energy-transport models for spin transport in ferromagnetic semiconductors

8/2016 *C. Abert, M. Ruggeri, F. Bruckner, C. Vogler, A. Manchon, D. Praetorius, and D. Suess*
Predicting giant magnetoresistance using a self-consistent micromagnetic diffusion model

7/2016 *B. Düring, A. Jüngel, and L. Trussardi*
A kinetic equation for economic value estimation with irrationality and herding

6/2016 *M. Amrein, J.M. Melenk, and T.P. Wihler*
An hp-adaptive Newton-Galerkin finite element procedure for semilinear boundary value problems

5/2016 *M. Gualdani and N. Zamponi*
Spectral gap and exponential convergence to equilibrium for a multi-species Landau system

Institute for Analysis and Scientific Computing
Vienna University of Technology
Wiedner Hauptstraße 8–10
1040 Wien, Austria

E-Mail: admin@asc.tuwien.ac.at
WWW: http://www.asc.tuwien.ac.at
FAX: +43-1-58801-10196

ISBN 978-3-902627-05-6

ASC TU WIEN

Spurious modes of the complex scaled Helmholtz Equation*

Lothar Nannen Markus Wess

July 20, 2016

Abstract

In this paper we study resonance problems in unbounded domains using a radial complex scaling method (frequently called perfectly matched layer method). The main focus of attention is given to artificial or spurious resonances arising from discretization. We analyze the dependency of these artificial resonances with respect to the discretization parameters and the scaling function. This includes a frequency dependent complex scaling leading to a cubic eigenvalue problems. We show that such scalings reduce the artificial resonances generated by the discretization of the complex scaled exterior domain. Hence, they simplify the choice of the corresponding exterior discretization parameters.

1 Introduction

Time-harmonic acoustic wave propagation can be modelled by the Helmholtz equation (see e.g. [15]). For scattering problems we are typically interested in solutions to a given positive frequency and a given source. In the corresponding resonance problem we are looking for complex resonances with positive real part such that for these resonances the scattering problem is not uniquely solvable.

The real part of the resonance is the resonance frequency and the absolute value of the quotient of real and imaginary part is the quality factor. If the quality factor is large, the solution to the scattering problem is very sensitive to external sources in the neighborhood of the resonance frequency (see [10]). Therefore, the computation of scattering resonances is of great

*The authors acknowledge support from the Austrian Science Fund (FWF): P26252.

interest, not only for acoustic problems, but e.g. for laser cavities and x-ray resonators [23] as well.

Typically, such problems are posed on unbounded domains. Hence, standard finite element methods are not directly applicable. One popular approach are boundary element methods ([27, 22]). They reduce the problem to the boundary of a given scatterer using the fundamental solution to the Helmholtz equation. Since the fundamental solution depends highly non-linear on the frequency, this results in non-linear eigenvalue problems. Even though such problems can be solved using the contour integral method [4], for resonance problems it is often more convenient to solve linear eigenvalue problems.

Therefore, we split the unbounded domain into a bounded interior domain and an unbounded exterior domain. While for the bounded interior problem standard finite elements can be used, the exterior domain needs particular attention. One relatively new method is the Hardy space infinite element method [12, 9]. For this method generalized radial coordinates are used to discretize the exterior problem using unbounded pyramidal frustums. Subsequently a Galerkin method with tensor product elements built by radial infinite elements and standard finite elements on the interface between the interior and the exterior domain is used. Since the basis functions are indepedent of the frequency, after discretization resonance problems transform to linear eigenvalue problems. Moreover, super-algebraic convergence with respect to the number of unknowns in radial direction is shown.

Nevertheless, the theoretical framework of this method is challenging and a non-standard infinite element has to be implemented in a finite element code. Since in some cases the Hardy space infinite element method is closely related to the complex scaling method (see [13] for cylindrical waveguide problems), in this paper, we focused on the latter method.

The complex scaling method was introduced amongst others by Simon in the 70s (see [26] or the reviews in [11, 20]). Roughly speaking for this method the real coordinates are stretched into the complex domain such that the imaginary part of the complex coordinates grow at least linearly with increasing distance to the interior domain. Since solutions to the Helmholtz equation on this complex manifold are exponentially decreasing, a truncation of the unbounded exterior domain into a bounded layer leads to an exponentially decreasing modelling error. Now this bounded layer can be discretized using standard finite element methods.

In 1994 Berenger [2] introduced the popular name perfectly matched layer method for essentially the same method (see [6]). Complex scaling is thereby regarded as an artificial absorbing layer such that no reflections at

the interface to the interior domain occur. For radial complex scaling convergence of the method was established in [7, 19, 14, 5] under some constraints on the complex damping function. In [3] a truncation free complex scaling was introduced using singular damping functions. Convergence of the corresponding resonance problems is studied in [17] or in [13] for cylindrical waveguide problems.

The main drawback of the complex scaling method is the amount of discretization parameters. In order to gain an optimal discretization, the finite element discretizations of the interior and the truncated exterior domain, the thickness of the damping layer, and the slope and the starting point of the damping function have to be adapted to the specific problem. Moreover, the discretization leads to artificial resonances, which can be hard to distinguish from the correct ones (see [16]).

In this paper we study the dependency of these artificial or spurious resonances with respect to the discretization parameters in one and two dimensions. Moreover, we compare the results for frequency independent damping functions with those for frequency dependent ones. The latter are typically used for time dependent problems (see e.g. [7]) in order to guarantee a frequency independent decay of the complex scaled solution. Such scalings lead to cubic eigenvalue problems and are therefore more complicated to solve as the linear eigenvalue problems obtained by frequency independent scalings. Nevertheless, using a frequency dependent scaling reduces the spurious resonances generated by the discretization of the exterior domain a lot. Therefore it simplifies the choice of the damping function and the discretization of the exterior domain.

The rest of this paper is organized as follows: Radial complex scaling for Helmholtz resonance problems is introduced in Sec. 2. In Sec. 3 we formulate the corresponding eigenvalue problems. Sec.4 contains the numerical studies in a simple one-dimensional setting. Two dimensional problems are studied in Sec. 5 and a short conclusion completes the paper.

2 Settings

In this paper we study different effects of discretization of resonance problems. We will consider standard linear complex scaling as well as a frequency dependent complex scaling.

2.1 Resonance problem

Let $\Omega \subset \mathbb{R}^d$ with $d = 1, 2$ be an unbounded Lipschitz domain such that $\Omega_{\text{ext}} := \{\mathbf{x} \in \mathbb{R}^d : \|\mathbf{x}\| > R\} \subset \Omega$ and $\partial\Omega_{\text{ext}} \cap \partial\Omega = \emptyset$ for given $R > 0$. We separate Ω into the bounded interior domain $\Omega_{\text{int}} := \Omega \setminus \overline{\Omega_{\text{ext}}}$, the interface $\Gamma := \partial\Omega_{\text{ext}}$ and the exterior domain Ω_{ext}, i.e. $\Omega = \Omega_{\text{int}} \cup \Gamma \cup \Omega_{\text{ext}}$.

Moreover, let $p \in L^\infty(\Omega)$ be an almost everywhere non-negative potential with $p \equiv 1$ in $\overline{\Omega_{\text{ext}}}$. We are looking for eigenpairs $(\omega, u) \in \mathbb{C} \times H^1(\Omega_{\text{int}})$ with $\Re(\omega) > 0$ and $u \neq 0$ such that

$$-\Delta u = \omega^2 p\, u \qquad \text{in} \quad \Omega_{\text{int}}, \tag{1a}$$

$$\mathrm{B}\, u = 0 \qquad \text{on} \quad \partial\Omega, \tag{1b}$$

$$\nabla u \cdot \mathbf{n} = \mathrm{DtN}(\omega) u \qquad \text{on} \quad \Gamma. \tag{1c}$$

B is a trace operator on $\partial\Omega$, e.g. a Dirichlet trace operator $\mathrm{B}\, u := u|_{\partial\Omega}$ or a Neumann trace operator $\mathrm{B}\, u := \nabla u \cdot \mathbf{n}|_{\partial\Omega}$ with normal vector $\mathbf{n}$. The Dirichlet-to-Neumann operator $\mathrm{DtN}(\omega) : H^{1/2}(\Gamma) \to H^{-1/2}(\Gamma)$ can be constructed using radiating solutions to the exterior scattering problem.

For $\omega > 0$ and $f \in H^{1/2}(\Gamma)$ let $u_{\text{ext}} \in H^1_{\text{loc}}(\Omega_{\text{ext}})$ be a solution to

$$-\Delta u_{\text{ext}} - \omega^2 u_{\text{ext}} = 0 \qquad \text{in} \quad \Omega_{\text{ext}}, \tag{2a}$$

$$u_{\text{ext}} = f \qquad \text{on} \quad \Gamma. \tag{2b}$$

In one dimension ($d = 1$), such solutions are given by

$$u_{\text{ext}}(x) = C \exp(i\omega|x|) + D \exp(-i\omega|x|). \tag{3}$$

For $d = 2$ we use polar coordinates and decompose u_{ext} into

$$u_{\text{ext}}(\mathbf{x}) = \sum_{\nu=-\infty}^{\infty} u_\nu(\|\mathbf{x}\|)\Phi_\nu\left(\frac{\mathbf{x}}{\|\mathbf{x}\|}\right). \tag{4}$$

For the usual parametrization $\frac{\mathbf{x}}{\|\mathbf{x}\|}(\varphi) = \binom{\cos\varphi}{\sin\varphi}$ of the unit circle and with the two dimensional spherical harmonics $\Phi_\nu \circ \mathbf{x}/\|\mathbf{x}\|(\varphi) = \exp(i\nu\varphi)$, (2a) separates into the Bessel equations

$$-u_\nu''(r) - \frac{1}{r}u_\nu'(r) - \left(\omega^2 - \frac{\nu^2}{r^2}\right) u_\nu(r) = 0, \qquad r > R. \tag{5}$$

Solutions to (5) are $u_\nu(r) = C_\nu H^{(1)}_{|\nu|}(\omega r) + D_\nu H^{(2)}_{|\nu|}(\omega r)$ with the Hankel functions $H^{(1,2)}_{|\nu|}$ of the first and second kind.

u_{ext} is called outgoing, if and only if $D = 0$ in one dimension and $D_\nu = 0$, $\nu \in \mathbb{Z}$, for $d = 2$ (see e.g. [8]). Hence, for $\omega > 0$ we define the standard Helmholtz Dirichlet-to-Neumann operator $\mathrm{DtN}(\omega) : H^{1/2}(\Gamma) \to H^{-1/2}(\Gamma)$ as

$$\left(\mathrm{DtN}(\omega) f\right)(\mathbf{x}) := \begin{cases} i\omega f(\mathbf{x}), & d = 1 \\ \sum\limits_{\nu=-\infty}^{\infty} \frac{\omega \left(H_{|\nu|}^{(1)}\right)'(\omega R)}{H_{|\nu|}^{(1)}(\omega R)} (f(R\bullet), \Phi_\nu)_{L^2(\partial B_1)} \Phi_\nu\left(\frac{\mathbf{x}}{R}\right), & d = 2 \end{cases} \tag{6}$$

with $\mathbf{x} \in \Gamma$ and for all $f \in H^{1/2}(\Gamma)$. In two dimensions $\omega \mapsto \mathrm{DtN}(\omega)$ has a meromorphic extension to $\omega \in \mathbb{C} \setminus \mathbb{R}_{\leq 0}$. The poles are the roots (scaled with $1/R$) of the Hankel functions of the first kind. For $\nu \in \mathbb{Z}$ there exist ν roots with negative imaginary part (see [1, p. 373]). In one dimension $\omega \mapsto \mathrm{DtN}(\omega)$ is holomorphic.

So, except for the poles of the DtN-operator, the resonance problem (1) is well defined. Since the discrete set of poles of DtN scales with $1/R$, by choosing a suitable R we can always ensure that the problem is well defined in a sufficiently small neighborhood of a fixed $\omega \in \mathbb{C}$ with $\Re(\omega) > 0$.

There exists a continuation of a solution $u_{\text{int}} \in H^1(\Omega_{\text{int}})$ of (1) to $u \in H^1_{\text{loc}}(\Omega)$ by

$$u(x) := \begin{cases} u_{\text{int}}(-R) \exp(-i\omega(x+R)), & x < -R, \\ u_{\text{int}}(x), & x \in \Omega_{\text{int}}, \\ u_{\text{int}}(R) \exp(i\omega(x-R)) & x > R \end{cases} \tag{7a}$$

for $d = 1$ and

$$u(\mathbf{x}) := \begin{cases} u_{\text{int}}(\mathbf{x}), & \mathbf{x} \in \Omega_{\text{int}}, \\ \sum_{\nu=-\infty}^{\infty} (u_{\text{int}}|_\Gamma(R\bullet), \Phi_\nu)_{L^2(\partial B_1)} H_{|\nu|}^{(1)}(\omega\|\mathbf{x}\|) \Phi_\nu\left(\frac{\mathbf{x}}{\|\mathbf{x}\|}\right), & \mathbf{x} \in \Omega_{\text{ext}} \end{cases} \tag{7b}$$

for $d = 2$. By construction u satisfies the Helmholtz equation (1a) with $p \equiv 1$ in Ω_{ext}. Hence, u is holomorphic in all subdomains of Ω, where p is constant.

Using analytic Fredholm theory it can be shown, that for $p \equiv 1$ there exists only a discrete set of resonances to (1). The resonances have positive real part and negative imaginary part (see [28, §9] or [21, Sec. 3.3]). If $\Omega = \Omega_{\text{ext}}$, i.e. if we consider scattering on a sphere with Dirichlet boundary conditions at $\partial\Omega$, the resonances are the scaled roots of the Hankel functions.

2.2 Complex scaling

In two dimensions the Dirichlet-to-Neumann operator (6) cannot be used in a numerical method. Hence, (1c) is typically replaced by an approximation. There exist different kinds of such transparent boundary conditions. In the simplest case, the one dimensional DtN operator is used as a first order absorbing boundary condition. This is justified for positive frequencies $\omega > 0$ by the Sommerfeld radiation condition

$$\lim_{\|\mathbf{x}\|\to\infty} \sqrt{\|\mathbf{x}\|}\left(\partial_{\|\mathbf{x}\|} u_{\text{ext}}(\mathbf{x}) - i\omega u_{\text{ext}}(\mathbf{x})\right) = 0.$$

Unfortunately, the Sommerfeld radiation condition is not equivalent to the radiation condition defined by (6) for resonances of (1) with negative imaginary part. Due to the asymptotic behaviour of the Hankel functions (see [8, Sec. 3.4])

$$H_\nu^{(1,2)}(r) = \sqrt{\frac{2}{\pi t}} \exp\left(\pm i\left(t - \nu\frac{\pi}{2} - \frac{\pi}{4}\right)\right)\left(1 + \mathcal{O}\left(\frac{1}{r}\right)\right) \text{ for } r \to \infty, \quad (8)$$

the corresponding outgoing resonance functions are exponentially increasing for $\|\mathbf{x}\| \to \infty$. Therefore, the Sommerfeld radiation condition as well as the first order absorbing boundary condition leads to incoming resonance functions.

In this paper we use a complex scaling method as numerical realization of the DtN-operator. In principle, for most of these methods there exist three steps:

- formulation of a complex scaled resonance problem (see (13)),
- truncation of Ω to a bounded domain Ω_T (see (14)), and
- finite element discretization of $H^1(\Omega_T)$ (see (16)).

In this subsection we start with the first step.

For $R > 0$ and $\sigma \in \mathbb{C}$ with positive real and imaginary part we define the continuous damping function $\gamma_{\sigma,R} : \mathbb{R}_{\geq 0} \to \mathbb{C}$ by

$$\gamma_{\sigma,R}(r) := \begin{cases} r, & r \leq R \\ \sigma(r-R) + R, & r > R \end{cases}, \quad R > 0,\ \Re(\sigma),\ \Im(\sigma) > 0. \quad (9)$$

Based on this damping function we introduce a complex scaled variable

$$\hat{\mathbf{x}}_{\sigma,R}(\mathbf{x}) := \begin{cases} \frac{\gamma_{\sigma,R}(\|\mathbf{x}\|)}{\|\mathbf{x}\|}\mathbf{x}, & \mathbf{x} \neq 0 \\ 0, & \mathbf{x} = 0 \end{cases}, \quad (10)$$

for $\mathbf{x} \in \Omega \subset \mathbb{R}^d$. Since $\Im(\sigma) > 0$, we have $\hat{\mathbf{x}}_{\sigma,R} \in \{z \in \mathbb{C} : \Im(z) > 0\}^d$ for $\|\mathbf{x}\| > R$ and $\hat{\mathbf{x}}_{\sigma,R} = \mathbf{x}$ for $\|\mathbf{x}\| \leq R$. $\gamma_{\sigma,R}$ is for all $\|\mathbf{x}\| \neq R$ arbitrarily smooth with Jacobian $J_{\sigma,R}(\mathbf{x}) := \frac{\partial}{\partial \mathbf{x}} \hat{\mathbf{x}}_{\sigma,R}(\mathbf{x})$.

Using the holomorphic extension of $u|_{\Omega_{\text{ext}}} \in H^1_{\text{loc}}(\Omega_{\text{ext}})$ defined in (7) to $\{z \in \mathbb{C} : \Im(z) > 0\}^d$, we define the complex scaled function

$$\hat{u}_{\sigma,R} := u \circ \hat{\mathbf{x}}_{\sigma,R}. \tag{11}$$

Due to the asymptotic behaviour (8) of the Hankel functions, the representation (7) of the solution u in Ω_{ext}, and the definition of the damping (9) $\hat{u}_{\sigma,R}$ decays exponentially if and only if

$$\Im(\omega\sigma) > 0. \tag{12}$$

Due to the assumption $\Im(\sigma) > 0$ this is always the case for positive frequencies. For resonances $\omega \in \mathbb{C}$ of (1) with positive real and negative imaginary part, (12) is only satisfied if $\Im(\sigma)/\Re(\sigma)$ is sufficiently large.

Since the Hankel functions ($d = 2$) as well as the exponential function ($d = 1$) are holomorphic in $\mathbb{C} \setminus \mathbb{R}_{\leq 0}$, u defined in (7) solves the Helmholtz equation not only for x but also for the complex scaled coordinate $\hat{\mathbf{x}}_{\sigma,R}$. Thus, if we define for an eigenpair $(\omega, u_{\text{int}}) \in \mathbb{C} \times H^1(\Omega_{\text{int}})$ of (1) the complex scaled eigenfunction $\hat{u}_{\sigma,R}$ as in (11) and if (12) holds, then $(\omega, \hat{u}_{\sigma,R}) \in \mathbb{C} \times V$ solves the complex scaled resonance problem

$$\int_\Omega J_{\sigma,R}^{-T} \nabla u \cdot J_{\sigma,R}^{-T} \nabla v \, \det(J_{\sigma,R}) \, d\mathbf{x} = \omega^2 \int_\Omega p \, u \, v \, \det(J_{\sigma,R}) \, d\mathbf{x}, \quad v \in V. \tag{13}$$

For Neumann boundary conditions at $\partial\Omega$ we have $V = H^1(\Omega)$. Dirichlet boundary conditions have to be incorporated as usual into V. Note, that the complex scaled resonance function $u_{\sigma,R}$ is at least not holomorphic for $\{\mathbf{x} \in \mathbb{R}^d : \|\mathbf{x}\| = R\}$, since the scaling $\gamma_{\sigma,R}$ defined in (9) is not holomorphic there.

2.3 Discretization and truncation

(13) is still posed on the unbounded domain Ω and therefore not directly feasible for a finite element discretization. Thus, typically Ω is truncated to a finite domain $\Omega_T := \{\mathbf{x} \in \Omega : \|\mathbf{x}\| \leq T\}$. If (12) holds, then the resonance functions $\hat{u}_{\sigma,R}$ constructed out of eigenpairs to (1) are exponentially decaying and we expect the truncation error to be small if $T > R$ is large enough. Using Neumann boundary conditions for the truncation boundary $\partial\Omega_T \setminus \partial\Omega$,

we are looking for eigenpairs $(\omega_T, \hat{u}_{\sigma,R,T}) \in \mathbb{C} \times V_T$ of

$$\int_{\Omega_T} J_{\sigma,R}^{-T} \nabla u \cdot J_{\sigma,R}^{-T} \nabla v \, \det(J_{\sigma,R}) \, d\mathbf{x} = \omega^2 \int_{\Omega_T} p \, u \, v \, \det(J_{\sigma,R}) \, d\mathbf{x}, \quad v \in V_T \tag{14}$$

with $V_T := H^1(\Omega_T)$ for Neumann boundary conditions at $\partial\Omega$.

In the following we study the different effects of finite element discretization. Let $V_{\text{int}}^h \subset H^1(\Omega_{\text{int}})$ and $V_{\text{ext}}^h \subset H^1(\Omega_T \setminus \Omega_{\text{int}})$ be constructed such that the trace spaces on the interface $\Gamma = \overline{\Omega_{\text{int}}} \cap \overline{\Omega_{\text{ext}}}$ coincide, i.e. $\{f|_\Gamma : f \in V_{\text{int}}^h\} = \{f|_\Gamma : f \in V_{\text{ext}}^h\}$. We solve for eigenpairs $(\omega_{h_i,h_e}, u_{h_i,h_e}) \in \mathbb{C} \times V_{h_i,h_e}$ with

$$V_{h_i,h_e} := \left\{ f \in V_T : f|_{\Omega_{\text{int}}} \in V_{\text{int}}^{h_i} \wedge f|_{\Omega_T \setminus \Omega_{\text{int}}} \in V_{\text{ext}}^{h_e} \right\}, \tag{15}$$

$\Re(\omega_{h_i,h_e}) > 0$ and $u_{h_i,h_e} \neq 0$ of

$$\int_{\Omega_T} J_{\sigma,R}^{-T} \nabla u \cdot J_{\sigma,R}^{-T} \nabla v \, \det(J_{\sigma,R}) \, d\mathbf{x} = \omega^2 \int_{\Omega_T} p \, u \, v \, \det(J_{\sigma,R}) \, d\mathbf{x}, \quad v \in V_{h_i,h_e}. \tag{16}$$

In our numerical tests, we choose different parameters T, h_i and h_e to show the different discretization effects. In particular we study the effects of

D.a discretization of the interior domain (h_e small and T large),

D.b truncation (reasonable $T > R$, h_i and h_e sufficiently small),

D.c discretization of the interior domain and truncation (h_e small),

D.d discretization of the truncated exterior domain (h_i small), and

D.e full discretization and truncation.

Additionally, we study the effects of the damping profile, i.e. the effects of the parameters σ and R. In contrast to standard implementations of resonance problems, we consider constant damping σ as well as a frequency dependent damping $\sigma = \sigma_0/\omega$. Similar damping profiles are widely used for time dependent problems (see e.g. [7]) in order to reduce the dependency of the truncation error with respect to the frequencies ω. For resonance problems, the Jacobian in (13) becomes a rational function in ω leading to a non-linear eigenvalue problem. Therefore, for resonance problems usually frequency independent scalings are used.

Since the spectral properties of frequency dependent dampings are quite promising, we also study such scalings. The resulting non-linear resonance problem is solved by linearization (see Sec. 3.2).

3 The frequency dependent complex scaled Helmholtz problem

In this section we deal with the (non-linear) eigenvalue problems resulting from (13) and the use of frequency dependent scaling functions $\sigma(\omega)$.

3.1 The essential spectrum

Definition 3.1. Let $T(\omega) : D \subset X \to X$ be a family of densely defined linear operators on some Banach space X, then we write

$$\Sigma(T) := \{\omega \in \mathbb{C} : T(\omega) \text{ is not boundedly invertible}\}. \tag{17}$$

As usual we can decompose $\Sigma(T)$ into two disjoint subsets

$$\Sigma(T) = \Sigma_{ess}(T) \dot{\cup} \Sigma_d(T), \tag{18}$$

where $\Sigma_d(T) := \{\omega \in \mathbb{C} : \omega \text{ is an eigenvalue of finite algebraic multiplicity}\}$.

Let $L_{\sigma,R}(\omega)$ be the $L^2(\Omega)$-closure of the operator

$$u \mapsto -\left(J_{\sigma,R}^{-T}\nabla\right) \cdot J_{\sigma,R}^{-T}\nabla u - \omega^2 p u. \tag{19}$$

Then $L_{\sigma,R} : \mathrm{dom}(L_{\sigma,R}) \subset L^2(\Omega) \to L^2(\Omega)$ is an (unbounded) operator and (13) is a weak form of the eigenvalue problem $L_{\sigma,R}(\omega)\, u = 0$.

For a frequency independent scaling $\sigma(\omega) \equiv \sigma_0$, in [11] it is shown that $\Sigma_{ess}(L_{\sigma,R}) = \left\{\omega \in \mathbb{C} : \arg \omega^2 + 2 \arg \sigma = 0\right\}$ for $\Omega = \mathbb{R}^n$. Restricted to ω with positive real part this is equivalent to $\Im(\sigma\omega) = 0$ (confer with (12)).

By a similar reasoning as in [18, Thm. 4.6] one can show that the essential spectrum does not change for $\Omega = \mathbb{R}^n \setminus \Omega_0$ and compact Ω_0. By the same reasoning, or alternatively by using compact perturbation theory, one can see, that $\Sigma_{ess}(L_{\sigma,R})$ is independent of the potential function p as well, since p has compact support by assumption.

For a frequency dependent scaling of the form $\sigma(\omega) = \sigma_0/\omega$ with $\Im(\sigma_0) > 0$, $L_{\sigma,R}(\omega)$ is in contrast to a frequency independent scaling non-linear in ω^2. Nevertheless, we can use the preceding results for the linear eigenvalue problem to show, that for $\omega \neq 0$ the operator $L_{\sigma,R}(\omega)$ is either invertible or ω is an eigenvalue, since $\Im(\sigma(\omega)\omega) = \Im(\sigma_0) > 0$. In other words there is no essential spectrum for ω with positive real part.

3.2 Solving the non-linear eigenvalue problem

Plugging finite element basis function into problem (16) for frequency dependent $\sigma(\omega)$ leads to a discrete eigenvalue problem of the form

$$M(\omega) = 0, \tag{20}$$

where $M : \mathbb{C} \to \mathbb{C}^{k\times k}$ is some matrix valued function. Available numerical methods for treating discrete non-linear eigenvalue problems include the contour integral method for analytic M (see e.g. [4]) and reduction to a linear eigenvalue problem by substitution for rational problems of the form

$$0 = M(\omega) = \sum_{j=N_0}^{N_1} M_j \omega^j, \tag{21}$$

where $M_j \in \mathbb{C}^{k\times k}$ are coefficient matrices and $N_0 < N_1 \in \mathbb{Z}$. Unfortunately, for a frequency dependent complex scaling the discrete formulation (16) in two dimensions is in general not of the form (21), which makes straightforward reduction to a linear eigenvalue problem by substitution impossible. Even if the contour integration method makes the treatment of such an eigenvalue problem possible, it is still advantageous to apply it to rational eigenvalue problems, since evaluation of $M(\omega)$ is less expensive.

To obtain an eigenvalue problem of the form (21), we use test functions of the form

$$\tilde{v}(\mathbf{x}) := \begin{cases} v(\mathbf{x}), & \mathbf{x} \in \Omega_{\text{int}}, \\ \frac{\gamma_{\sigma,R}(\|\mathbf{x}\|)}{R} v(\mathbf{x}), & \mathbf{x} \in \Omega_{\text{ext}}. \end{cases} \tag{22}$$

Note that, since $0 \notin \Omega_{\text{ext}}$, the map defined by (22) is an automorphism on $H^1(\Omega_T)$.

Plugging test functions $\tilde{v}$ into (14) and using the identities

$$J^{-1}_{\sigma,R}(\mathbf{x}) = \frac{\|\mathbf{x}\|}{\gamma_{\sigma,R}(\|\mathbf{x}\|)} I + \left(\frac{1}{\|\mathbf{x}\|^2 \gamma'_{\sigma,R}(\|\mathbf{x}\|)} - \frac{1}{\|\mathbf{x}\| \gamma_{\sigma,R}(\|\mathbf{x}\|)} \right) \mathbf{x}\mathbf{x}^T, \tag{23}$$

$$\det J_{\sigma,R}(\mathbf{x}) = \frac{\gamma_{\sigma,R}(\|\mathbf{x}\|)\, \gamma'_{\sigma,R}(\|\mathbf{x}\|)}{\|\mathbf{x}\|}, \tag{24}$$

for $\mathbf{x} \in \Omega_{\text{ext}}$, gives after some calculations

$$A_{\text{int}}(u,v) + A_{\text{ext}}(u,v) = \omega^2 \left(B_{\text{int}}(u,v) + B_{\text{ext}}(u,v) \right), \tag{25}$$

with

$$A_{\text{int}}(u,v) := \int_{\Omega_{\text{int}}} \nabla u \cdot \nabla v \, d\mathbf{x}, \quad B_{\text{int}}(u,v) := \int_{\Omega_{\text{int}}} puv \, d\mathbf{x}, \tag{26}$$

and

$$A_{\text{ext}}(u,v) := \frac{1}{R}\int_{\Omega_{\text{ext}}} \left(\gamma'_{\sigma,R}(\|\mathbf{x}\|)\,\|\mathbf{x}\| + \frac{\gamma^2_{\sigma,R}(\|\mathbf{x}\|)}{\gamma'_{\sigma,R}(\|\mathbf{x}\|)\,\|\mathbf{x}\|^3} \right) \nabla u \cdot \nabla v \tag{27}$$

$$+ \frac{\gamma_{\sigma,R}(\|\mathbf{x}\|)}{\|\mathbf{x}\|^2}\nabla u \cdot \mathbf{x} v - \frac{\gamma'_{\sigma,R}(\|\mathbf{x}\|)}{\|\mathbf{x}\|}\nabla u \cdot \mathbf{x}\mathbf{x}^T \nabla v \, d\mathbf{x} \tag{28}$$

$$B_{\text{ext}}(u,v) := \int_{\Omega_{\text{ext}}} uv \frac{\gamma^2_{\sigma,R}(\|\mathbf{x}\|)\,\gamma'_{\sigma,R}(\|\mathbf{x}\|)}{R\|\mathbf{x}\|}\, d\mathbf{x}. \tag{29}$$

For a damping function $\gamma_{\sigma,R}(r) := \frac{\sigma_0}{\omega}(r-R)+R$, we obtain a rational eigenvalue problem of the form

$$\sum_{j=-1}^{3} \omega^j A_j(u,v) = 0 \tag{30}$$

with bilinear forms

$$A_{-1}(u,v) := \frac{\sigma_0}{R}\int_{\Omega_{\text{ext}}} \left(\|\mathbf{x}\| + \frac{(\|\mathbf{x}\|-R)^2}{\|\mathbf{x}\|^3} \right) \nabla u \cdot \nabla v \, d\mathbf{x}$$

$$+ \frac{\sigma_0}{R}\int_{\Omega_{\text{ext}}} \frac{\|\mathbf{x}\|-R}{\|\mathbf{x}\|^2}\mathbf{x}\cdot\nabla u\, v\, d\mathbf{x} - \frac{\sigma_0}{R}\int_{\Omega_{\text{ext}}} \frac{1}{\|\mathbf{x}\|}\nabla u \cdot \mathbf{x}\mathbf{x}^T\nabla v\, d\mathbf{x}$$

$$- \frac{\sigma_0^3}{R}\int_{\Omega_{\text{ext}}} \frac{(\|\mathbf{x}\|-R)^2}{\|\mathbf{x}\|} uv\, d\mathbf{x} \tag{31a}$$

$$A_0(u,v) := \int_{\Omega_{\text{int}}} \nabla u \cdot \nabla v\, d\mathbf{x} + 2\int_{\Omega_{\text{ext}}} \frac{\|\mathbf{x}\|-R}{\|\mathbf{x}\|^3}\nabla u\cdot\nabla v\, d\mathbf{x}$$

$$+ \int_{\Omega_{\text{ext}}} \frac{1}{\|\mathbf{x}\|^2}\mathbf{x}\cdot\nabla u\, v\, d\mathbf{x} - 2\sigma_0^2\int_{\Omega_{\text{ext}}} \frac{\|\mathbf{x}\|-R}{\|\mathbf{x}\|} uv\, d\mathbf{x} \tag{31b}$$

$$A_1(u,v) := \frac{R}{\sigma_0}\int_{\Omega_{\text{ext}}} \frac{1}{\|\mathbf{x}\|^3}\nabla u\cdot\nabla v\, d\mathbf{x} - R\sigma_0\int_{\Omega_{\text{ext}}} \frac{1}{\|\mathbf{x}\|} uv\, d\mathbf{x} \tag{31c}$$

$$A_2(u,v) := -\int_{\Omega_{\text{int}}} puv\, d\mathbf{x}. \tag{31d}$$

Plugging in test and ansatz functions gives a rational eigenvalue problem (21) with matrices M_j arising from the respective bilinear forms (31).

4 Effects of discretization in one dimension

In this chapter we study the effects of the five steps of discretization (see Subsection 2.3) of Problem (1) or equivalently (13) in one dimension.

Let $\Omega_{\text{int}} := (0, R)$, $p_0 \geq 1$ and $R \geq R_0 > 0$ be given. Then we define the potential function by $p(x) := p_0^2 \chi_{[0,R_0]}(x)$, where χ_M denotes the characteristic function of a set M. Moreover we use Neumann boundary conditions at $\partial\Omega$, i.e. $u'(0) = 0$.

Using an ansatz

$$u(x) = \begin{cases} C_1 \exp(-ip_0\omega x) + C_2 \exp(ip_0\omega x), & x \in [0, R_0) \\ C_3 \exp(-i\omega x) + C_4 \exp(i\omega x), & x \in [R_0, R], \end{cases} \tag{32}$$

the exact DtN-Operator (6) and regularity of u at R_0, straightforward calculations show that the resonances of this one dimensional problem with positive real part are given by

$$\omega_k := \frac{1}{2p_0R_0} \left(-i \log\left(\frac{p_0 + 1}{p_0 - 1} \right) + 2k\pi \right), \; k \in \mathbb{N}, \tag{33}$$

for $p_0 > 1$ and that there are no resonances for $p_0 = 1$.

4.1 Discretization of the interior domain

In one dimension effects of the discretization of the interior domain can be easily studied by using a finite element approximation in Ω_{int} and the correct absorbing boundary condition. All the following results were obtained using finite element basis functions of polynomial order 6 with uniform mesh-size h.

Figure 1 shows the approximated resonances for different mesh-sizes h. The calculations exhibit a set of spurious interior resonances generated by the discretization. The approximation quality of the true resonances corresponds roughly with their distance to the interior spurious resonances. For smaller mesh-size h the curve connecting these resonances moves farther away from the real axis.

In Figure 2 the mesh-size h is kept constant, while the parameter R representing the location of the absorbing boundary is varied. Note, that for $R = R_0$ the spurious resonances vanish. The larger $R - R_0$ (i.e. the distance of the scatterer to the absorbing boundary), the less correct eigenvalues are calculated. This behaviour is a natural consequence of the fact, that the eigenfunctions are exponentially increasing in Ω_{int} (cf. Figure 3). So discretization errors generated in $[0, R_0]$ are amplified with increasing distance $R - R_0$.

Taking into account Figure 4b, we can conclude, that the relevant quantity for the location of the spurious resonances is indeed $R - R_0$. Figure

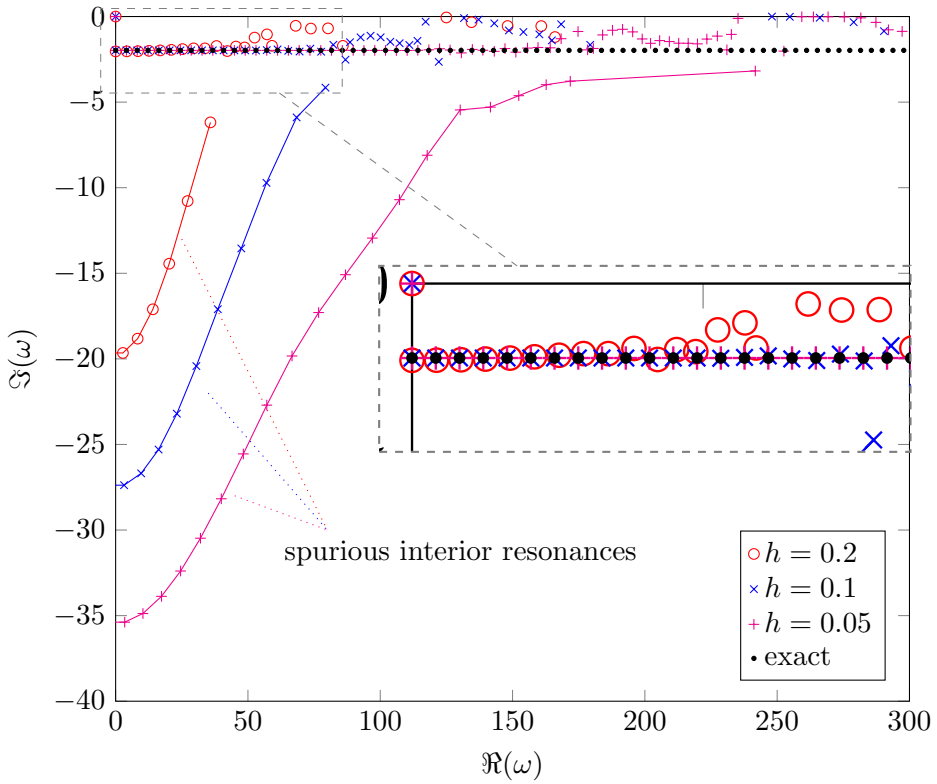

Figure 1: Resonances of the one-dimensional resonance problem for different mesh-sizes h, fixed potential $p_0 = 1.1$, $R_0 = 0.7$ and fixed boundary $R = 1$ with exact Dirichlet-to-Neumann operator.

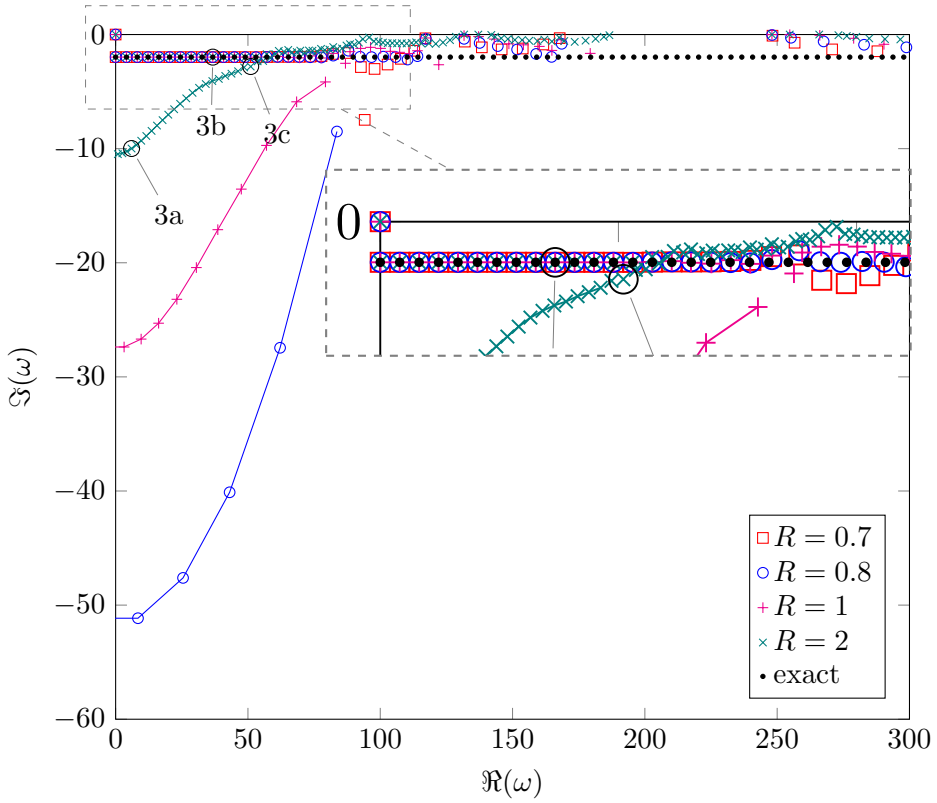

Figure 2: Resonances for fixed mesh-size $h = 0.1$ and fixed potential $p_0 = 1.1$, $R_0 = 0.7$ and with different boundaries R of the exact Dirichlet-to-Neumann operator.

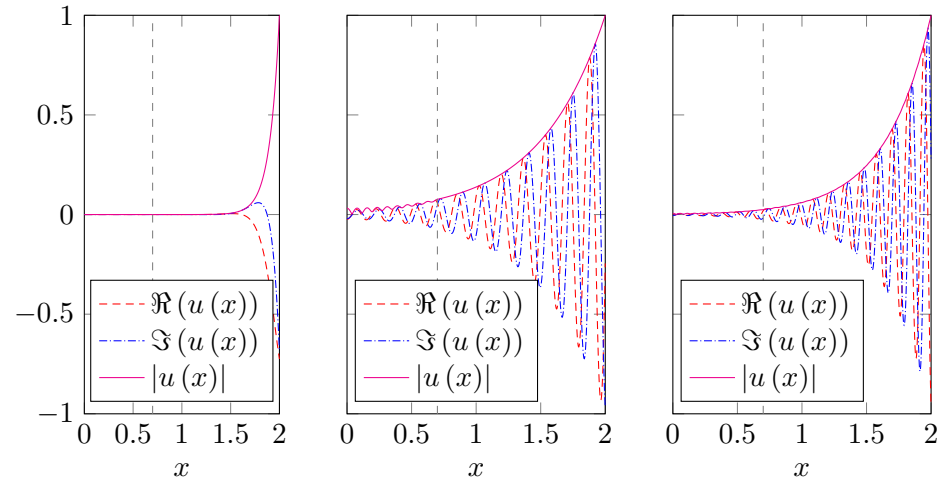

(a) $\omega \approx 6.0193 - 9.9883i$ (b) $\omega \approx 36.7223 - 1.9790i$ (c) $\omega \approx 51.0383 - 2.8031i$

Figure 3: Eigenfunctions u in Ω_{int} corresponding to selected resonances ω from Figure 2. The vertical dashed line marks the jump in the potential function p.

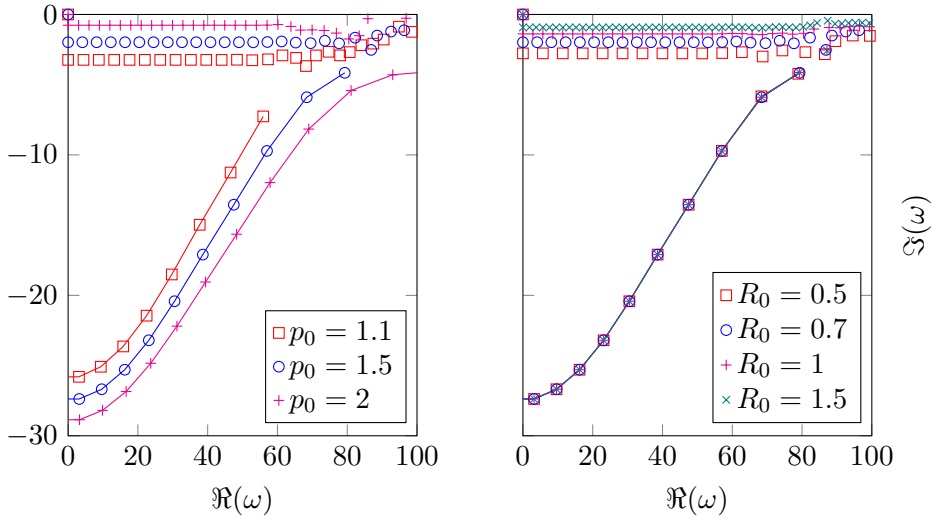

(a) $R_0 = 0.7$, $R = 1$ (b) $R = R_0 + 0.3$, $p_0 = 1.1$

Figure 4: Resonances for fixed mesh-size $h = 0.1$ and different potentials p_0, R_0 and boundaries R of the exact Dirichlet-to-Neumann operator.

3 shows three eigenfunctions corresponding to eigenvalues from Figure 2. While 3b is a correct resonance, the functions in 3c and 3a correspond to spurious resonances. Note, that distinguishing the spurious from the correct resonances by the shape of the eigenfunctions seems to be impossible in this example.

All in all we can conclude, that in this example spurious resonances are generated already by discretization of the interior domain, if $R - R_0 > 0$. Their location depends heavily on $R - R_0$ and h (cf. Figures 1, 2 and 4b) and to a lesser extent on the potential parameter p_0 (cf. Figure 4a). In the following we will refer to these spurious resonances as interior spurious resonances.

4.2 Truncation

Let $T > R$ and $\Omega_T := (0, T) = \Omega_{\text{int}} \cup \Gamma \cup \Omega_{\text{pml}}$, where $\Omega_{\text{int}} := (0, R)$, $\Gamma := \{R\}$, and $\Omega_{\text{ext}} := (R, T)$. If we prescribe Neumann boundary conditions at $\{0, T\}$, the resonances of (14) can be calculated using a similar ansatz to (32) and are solutions of the equation

$$p_0 \tan(p_0 R\omega) + \tan((T - R)\sigma\omega) = 0. \tag{34}$$

We use the two different scalings of the form (9) with

$$\sigma_1(\omega) :\equiv \sigma_0, \tag{35}$$

$$\sigma_2(\omega) := \frac{\sigma_0}{\omega}, \tag{36}$$

for $\sigma_0 \in \mathbb{C}$. With $p_0 = 1$ this leads to resonances

$$\omega_{k,T}^{\sigma_1} = \frac{\frac{k\pi}{T}}{\frac{R(1-\sigma_0)}{T} + \sigma_0}, \qquad k \in \mathbb{Z}, \tag{37a}$$

$$\omega_{k,T}^{\sigma_2} = -\frac{\sigma_0(1 - \frac{R}{T}) + \frac{k\pi}{T}}{\frac{R}{T}}, \qquad k \in \mathbb{Z} \setminus \{0\}, \tag{37b}$$

respectively. As mentioned earlier for $p_0 = 1$ there are no correct resonances. The resonances (37a) are a discretization of the essential spectrum, since $\{\omega_k^{\sigma_1} : k \in \mathbb{Z}\} \to \{\omega \in \mathbb{C} : \arg(\omega^2\sigma_0^2) = 0\}$ for $T \to \infty$ (cf. 3.1). The resonances (37b) diverge for $T \to \infty$. Both of them will be referred to as truncation resonances. Note, that $\Im\left(\omega_{k,T}^{\sigma_2}\right) = \Im(\sigma_0)\left(1 - \frac{T}{R}\right) < 0$ is constant for all $k \in \mathbb{Z} \setminus \{0\}$.

By the implicit function theorem, we can conclude, that this behaviour of the truncation resonances is also valid for $p_0 \approx 1$, although in this case there are additional correct resonances of (1).

4.3 Discretization of the interior domain and truncation

We study the effects of discretization of the interior domain and truncation using basis functions of order 10 in the exterior domain and again of order 6 in the interior domain. Figure 5 shows the effects of varying different parameters for scalings σ_1, σ_2 as defined in Section 4.2.

Two kinds of artificial resonances can be observed: The truncation resonances from (37a) and (37b) and the interior spurious resonances (cf. Section 4.1). More precisely, for the frequency dependent scaling we see only the truncation resonances above the interior spurious resonances and for the constant scaling we see only the interior spurious resonance above the truncation resonances.

Note that the interior spurious resonances are almost independent of the type of scaling and the parameters σ_0, $T-R$. They are merely a result of the discretization of the interior domain. As indicated by (37b) the truncation resonances in the frequency dependent case move away from the real axis for growing $\Im(\sigma_0)$. For the constant scaling we see almost straight rays starting from the origin and depending on $\arg(\sigma_0)$ as expected by (37a).

So overall, the classification of artificial resonances in truncation or interior spurious resonances is justified in this case.

4.4 Discretization of the truncated exterior domain

Using basis functions of order 10 in the interior domain and of order 5 in the exterior domain gives us a chance to study the effects of the discretization of the truncated exterior domain only. Figure 6 shows spurious resonances generated by the discretization of the truncated exterior domain. For the frequency independent complex scaling the exterior spurious resonances are located on a curve shaped similarly as the one containing the interior spurious resonances but much closer to the origin. The interior spurious resonances, indicated by the green line are no longer present, since their location would be below the exterior spurious resonances.

Comparison of the eigenvalues for $\sigma_0 = 1 + 5i, 1 + 10i$ in Figures 5b, 5d and 6b, 6d leads to the conclusion, that exterior spurious resonances in the frequency scaled case are located on horizontal lines, similar to the truncation resonances. With increasing mesh-size h_{ext} they move away from the truncation resonances and closer to the real axis. This shift is larger for larger values of $\Im(\sigma_0)$ and mesh-size. E.g. for $\sigma_0 = 1+5i$ and $h_{\text{ext}} = 0.1, 0.2$ as well as for $\sigma_0 = 1 + 10i$ and $h_{\text{ext}} = 0.1$ there is no shift and thus the exterior spurious resonances equal the truncation resonances.

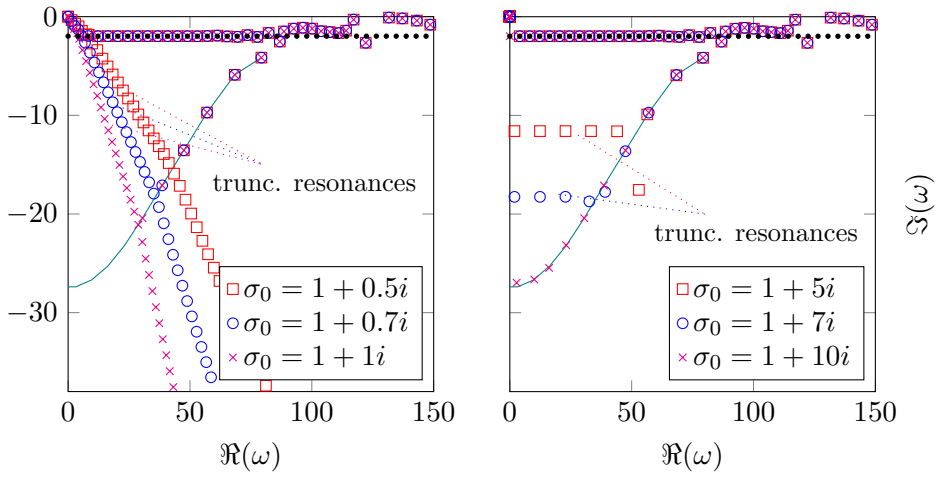

(a) $\sigma \equiv \sigma_0$, $h_{\text{int}} = 0.1$

(b) $\sigma = \frac{\sigma_0}{\omega}$, $h_{\text{int}} = 0.1$

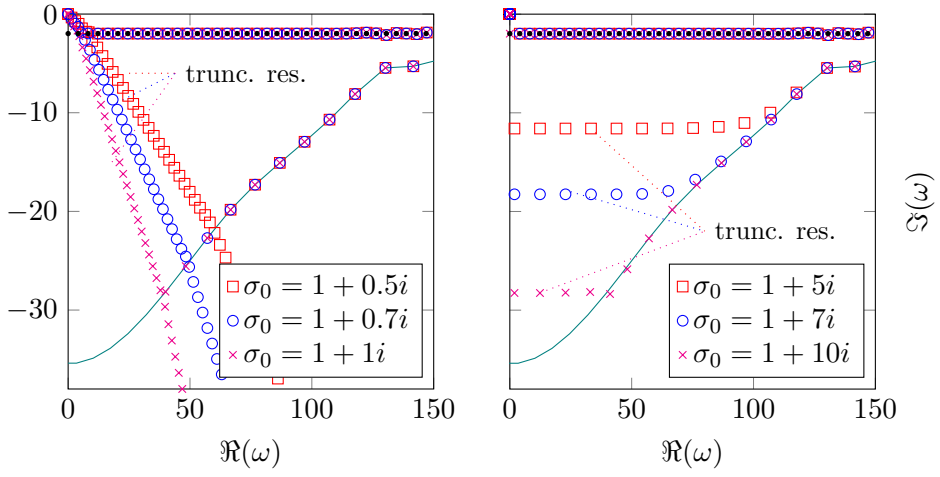

(c) $\sigma \equiv \sigma_0$, $h_{\text{int}} = 0.05$

(d) $\sigma = \frac{\sigma_0}{\omega}$, $h_{\text{int}} = 0.05$

Figure 5: Resonances for different complex scalings with very fine exterior discretization. Exact resonances are represented as black dots and the teal line marks the location of the interior spurious resonances calculated with exact absorbing boundary conditions (cf. Section 4.1)

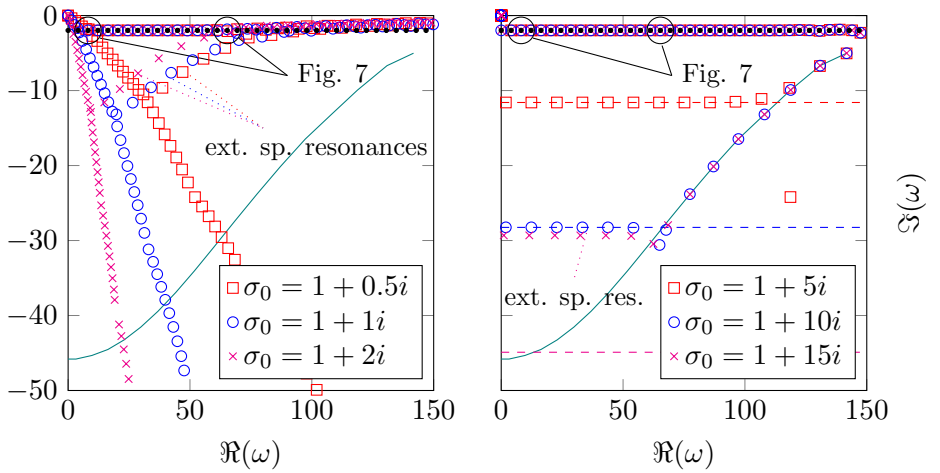

(a) $\sigma \equiv \sigma_0$, $h_{\text{ext}} = 0.1$

(b) $\sigma = \frac{\sigma_0}{\omega}$, $h_{\text{ext}} = 0.1$

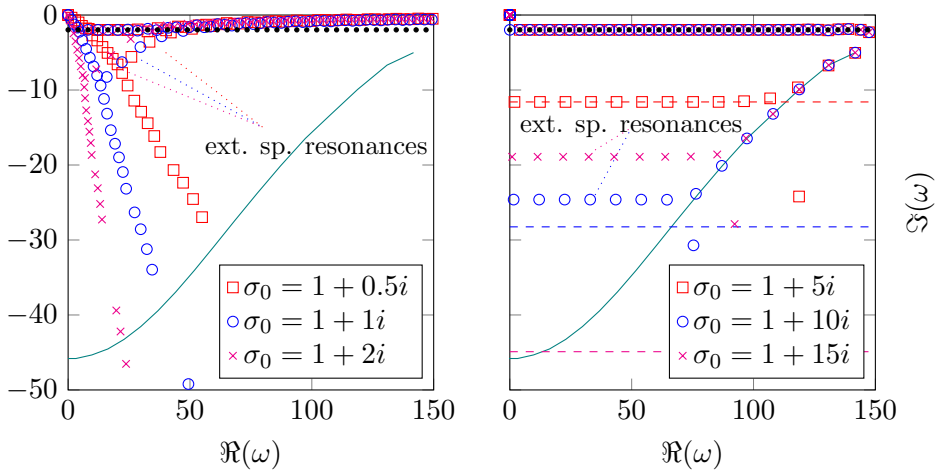

(c) $\sigma \equiv \sigma_0$, $h_{\text{ext}} = 0.2$

(d) $\sigma = \frac{\sigma_0}{\omega}$, $h_{\text{ext}} = 0.2$

Figure 6: Resonances for different complex scalings with coarse exterior discretization. Exact resonances are represented as black dots and the teal line marks the location of the interior spurious resonances calculated with exact absorbing boundary conditions (cf. Section 4.1). The horizontal dashed lines in the frequency scaled case show the locations of the truncation resonances (cf. Section 4.2)

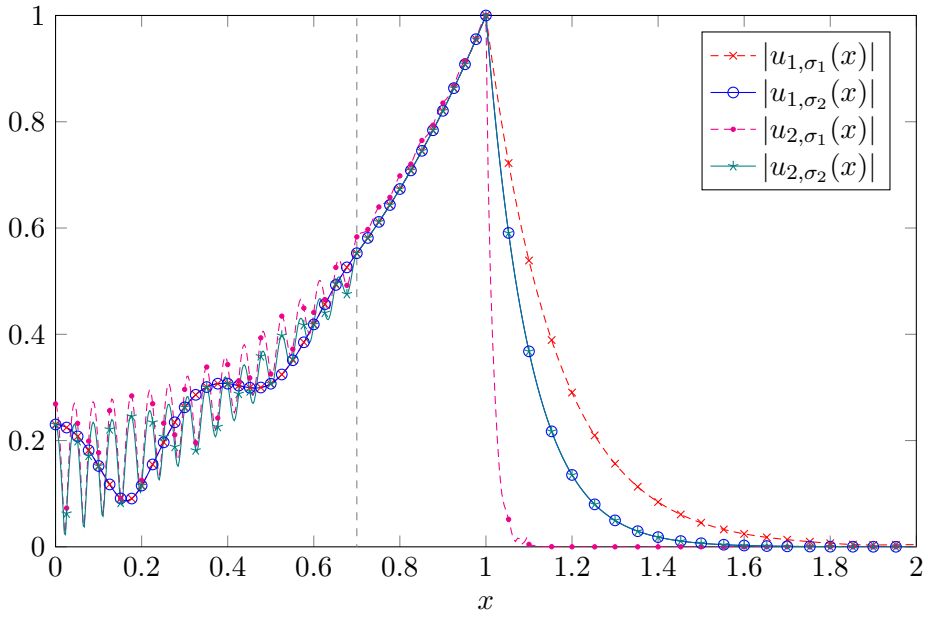

Figure 7: Absolut value of approximated eigenfunctions corresponding to $\omega_1 \approx 8.1599 - 1.9769i$, $\omega_2 \approx 65.2798 - 1.9769i$ with scaling functions $\sigma_1(\omega) \equiv 1 + i$, $\sigma_2(\omega) = \frac{1+10i}{\omega}$

Since the imaginary parts of the spurious exterior resonances are constant in all cases, they do not pollute the correct resonances of (1) near the real line. This dependency is less critical as the one in the constant scaling case, where with the same discretization much less correct resonances of (1) can be computed.

In both, frequency dependent and frequency independent complex scaling the location of the exterior spurious resonances depends only on the damping parameter σ_0, the exterior mesh-size h_{ext} and is independent of the diameter of the complex scaled domain $T - R$

Due to (7) the absolute values of the resonance functions of (1) are given in the complex scaled domain by $\exp(-\Im(\omega\sigma)x)$. Thus, for the frequency depending scaling $\sigma = \sigma_0/\omega$ the exponential decay is independent of the frequency. For the frequency independent scaling the resonance functions may decay to slow ($\Im(\omega\sigma_0)$ to small) resulting in large truncation errors or to fast ($\Im(\omega\sigma_0)$ to large) resulting in large approximation errors. The latter is the explanation for the worse results of the frequency independent scaling in Figures 6a and 6c.

4.5 Full discretization and truncation

As described in the previous sections, in one dimension there are three kinds of spurious resonances: the discretization of the essential spectrum generated by truncation (cf. Section 4.2), interior spurious resonances (cf. Sections 4.1 and 4.3) and exterior spurious resonances (cf. Section 4.4). In all the simulations, the interior spurious resonances are located on a curve connecting the negative imaginary axis with the positive real axis.

For the classical complex scaling with $\sigma \equiv \sigma_0$, the discretization of the essential spectrum is a subset of a straight line through the origin and the exterior spurious resonances lie on a similar curve as the interior ones but closer to the origin.

For the frequency dependent version $\sigma = \frac{\sigma_0}{\omega}$, the truncation resonances and the exterior spurious resonances are subsets of straight lines, parallel to the real axis.

In all cases, true resonances can only be found in the smallest region bounded by the positive real axis, the negative imaginary axis and the curves containing the truncation and various spurious resonances. If for a given set of parameters resonances outside this region are sought, e.g. resonances near the real axis with larger real part, it is not a priori clear which parameters have to be adapted.

For the frequency dependent scaling the preceding results indicate, that

most often the discretization of the interior domain needs to be refined. Exterior spurious resonances near the real axis are only an issue, if the exterior discretization is very coarse in comparison to the interior one or if $\Im(\sigma_0)$ is very small.

For frequency independent scalings the situation is more involved. Fig. 6 shows, that it can easily happen that the choice of σ_0 or of the exterior discretization is responsible for poor results. So one can see the frequency dependent scaling as an easy to use optimal choice of the exterior discretization, where the price to pay is the need to solve a polynomial eigenvalue problem.

5 Effects of discretization in two dimensions

In this section we follow up our studies of the one dimensional case in the previous section by analyzing two dimensional examples. Since it is closely related to the Helmholtz equation in one dimension, we start off with an example that can simplified to the one dimensional Bessel equations followed by a two dimensional example, where separation is not possible.

5.1 Bessel equations

In the following, we consider Problem (13) with $\Omega_{\text{int}} := B_R(0) \setminus B_{R_0}(0)$, for $R > R_0 > 0$ and $p(\mathbf{x}) \equiv 1$. In this case, the resonances are the roots of the functions

$$r \mapsto \left(H_\nu^{(1)}\right)'(R_0 r)\,, \quad \nu = 0, 1, \ldots \tag{38}$$

and can be computed semi-analytically.

Using a separation ansatz as in Section 2, this problem simplifies to the one dimensional Bessel equations (5). Applying a transformation $\tilde{u}_\nu(r) := \sqrt{r + R_0}u_\nu(r)$ leads to the equivalent formulation

$$-\tilde{u}_\nu''(r) - \left(\omega^2 - \frac{\nu^2 - \frac{1}{4}}{(r + R_0)^2}\right)\tilde{u}_\nu(r) = 0, \tag{39}$$

where homogeneous Neumann boundary values are transformed into Robin boundary conditions

$$\tilde{u}_\nu'(r)\, r + \frac{1}{2}\tilde{u}_\nu(r) = 0. \tag{40}$$

Thus, the Bessel equations can be interpreted as a continuous perturbation in the index ν of the one dimensional Helmholtz equation. Figures 8 and 9

show approximated and exact eigenvalues of Bessel equations with different indices using classical and frequency dependent complex scaling with same mesh and polynomial order.

In the classical case we can observe truncation and exterior spurious resonances, as in the one dimensional case (cf. Sections 4.2, 4.4) which depend also on the Bessel index ν. The truncation resonances for a fixed index ν are still located on a straight line resulting in a sector of truncation resonances for multiple indices ν. The more problematic exterior spurious resonances again behave like in the one dimensional case for fixed ν and move closer to the real axis for larger index ν. The green line marks the location of the interior spurious resonances in the one dimensional case. Due to the location of the exterior spurious resonances no interior ones are calculated in this example.

So for the classical complex scaling resonances with absolute values up to around 16 are approximated properly for the chosen mesh-size, thickness of the damping layer and damping factor σ. In this case the limiting factor is the location of the exterior spurious resonances. Although these depend on the choice of the damping $\sigma = 1+2i$ (confer with Fig. 6a), in all our computations using different damping factors the exterior spurious resonances stayed the limiting factor for the computations of the correct resonances. So a finer discretization of the exterior domain and/or a different thickness of the damping layer is needed to obtain better results.

In the case of the frequency dependent complex scaling we can observe truncation/exterior and interior spurious resonances known from the one dimensional case. Again for fixed index ν both of them behave like in the one dimensional case. For larger index ν the truncation/exterior spurious resonances move upwards, but their imaginary part stays bounded away from zero resulting in a horizontal strip. Thus, the truncation/exterior spurious resonances do not interfere with the approximated real resonances. The interior spurious resonances behave like the exterior spurious resonances in the classical case and move towards the real axis for growing ν. Additionally we can observe another set of spurious resonances located near the origin and the imaginary axis.

For the frequency depending complex scaling resonances with absolute values up to around 32 are approximated properly. In this case the limiting factor are the interior spurious resonances, which depend on the discretization of the interior domain. So here an optimization of the exterior discretization or the chosen complex scaling would not lead to any improvement.

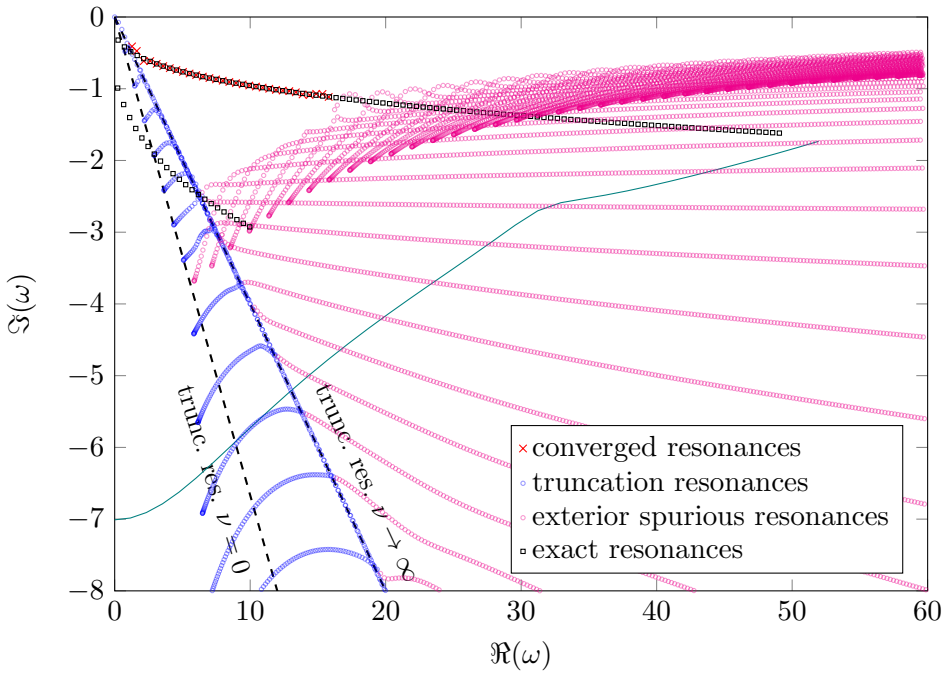

Figure 8: Approximated resonances of Bessel equations with indizes $\nu = 0, \ldots, 100$, $\Omega_{\text{int}} = [2, 4]$, $\Omega_{\text{ext}} = [4, 5]$, $\sigma(\omega) = 1 + 2i$

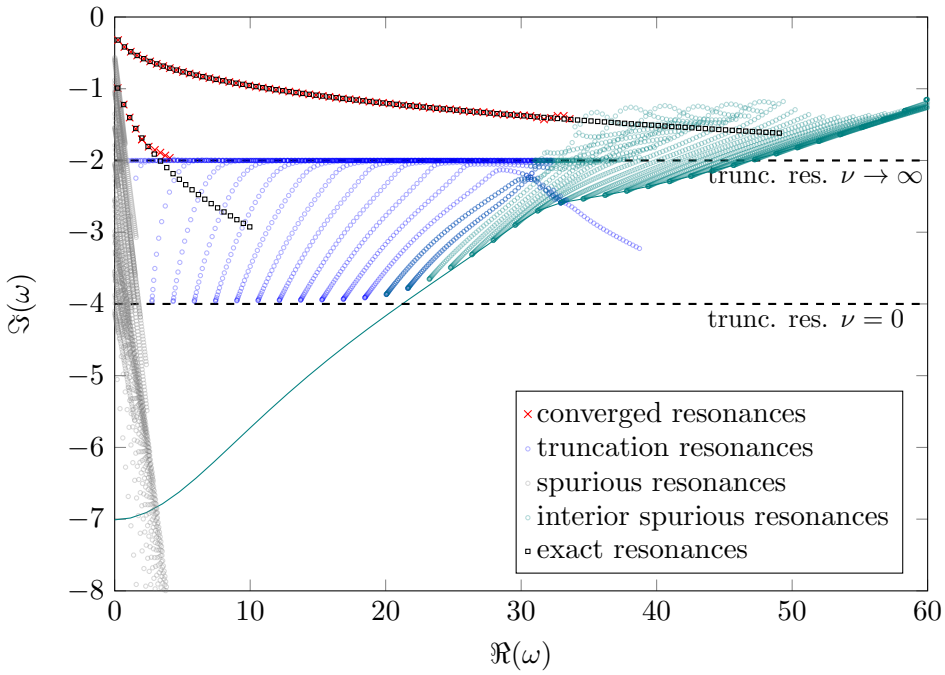

Figure 9: Approximated resonances of Bessel equations with indices $\nu = 0, \ldots, 100$, $\Omega_{\text{int}} = [2, 4]$, $\Omega_{\text{ext}} = [4, 5]$, $\sigma(\omega) = \frac{10+8i}{\omega}$

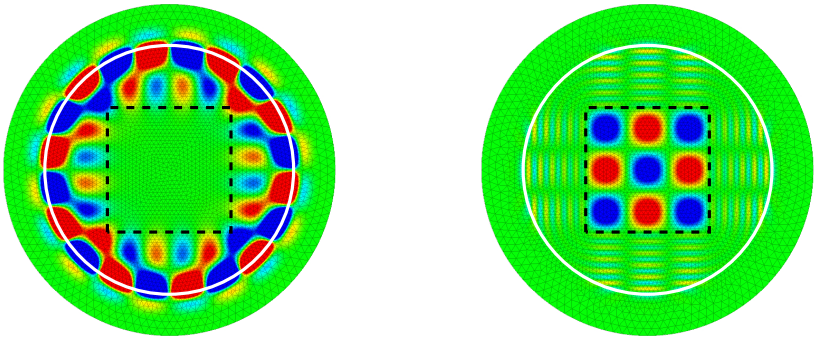

(a) $\omega \approx 4.90236 - 1.63113i$. (b) $\omega \approx 22.2143 - 0.67805i$

Figure 10: Real part of resonance functions of the two dimensional problem (cf. Figure 12). The dashed square marks the jump in the potential, and the white circle the boundary between Ω_{int} and Ω_{ext}.

5.2 Full two dimensional case

Finally, we study a full two dimensional problem using the high-order finite element implementation Netgen/NGSolve ([24], [25]). Due to the lack of rotational symmetry in this example no separation as in Sec. 5.1 is possible. We choose $\Omega_{\text{int}} := B_3(0)$, $\Omega_{\text{ext}} := B_4(0) \setminus \overline{B_3(0)}$ and $p(\mathbf{x}) = 1 - 0.8\chi_{[-2,2]^2}(\mathbf{x})$. Figures 11 and 12 show resonances calculated with standard and frequency dependent complex scaling. We find a kind of scattering resonances, that are perturbations of the roots of the Hankel functions and depend mainly on the volume $\partial[-2,2]^2$ of the "scatterer" (cf. Figure 10a). Moreover we find a set of transmission resonances with imaginary part approximately -0.7 and increasing real part (cf. Figure 10b).

Focusing on spurious resonances, we can observe the same effects as we saw studying the Bessel equations: In the frequency independent case (Figure 11) we see truncation resonances and exterior spurious resonances. In the frequency dependent case (Figure 12) we observe truncation and interior spurious resonances. Also the additional resonances near the imaginary axis can be observed. All of the aforementioned spurious resonances behave similarly as the ones of the Bessel equations, in the frequency independent as well as in the frequency dependent case.

Again the frequency dependent complex scaling produces a larger quan-

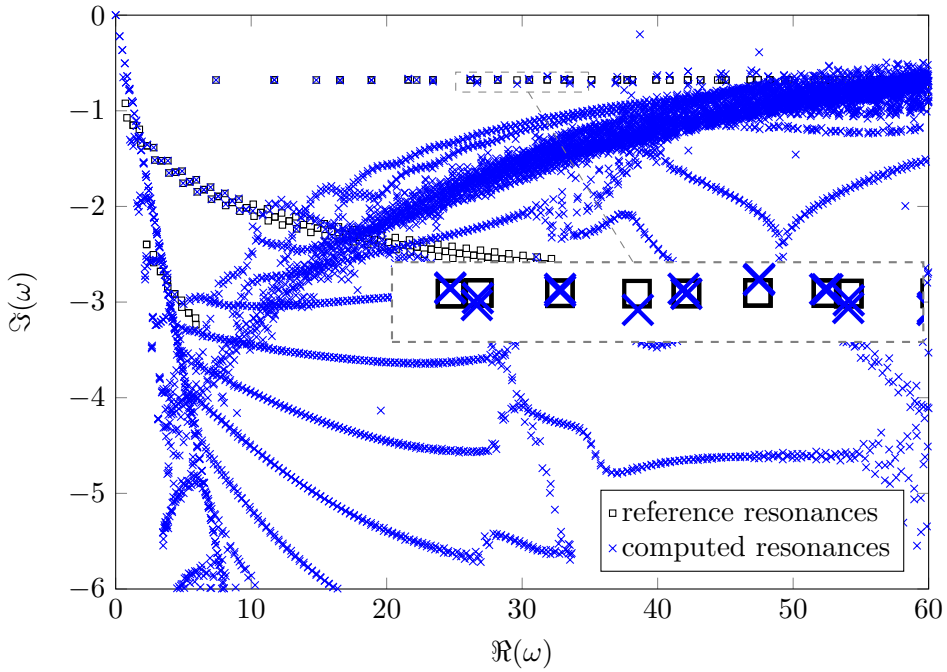

Figure 11: Computed resonances of a two dimensional resonance problem using classical complex scaling with $\sigma(\omega) \equiv 1 + 3i$. The reference resonances where calculated using higher polynomial order.

tity of correct resonances as the frequency independent complex scaling does, since in the frequency independent case the exterior spurious resonances pollute the domain of interest. So all remarks to the one-dimensional results remain valid for this two dimensional problem.

6 Conclusion and Outlook

In this paper we have studied the effects of the various parameters and sub-steps in the discretization process of a complex scaling method on the computed resonances of the Helmholtz equation in one and two dimensions. We have classified the occurring spurious resonances into truncation resonances, which are an approximation to the essential spectrum and interior and exterior spurious resonances, generated by discretization of the interior and exterior domain respectively. In applications, where resonances near the real axis are sought-after, the interior and exterior spurious resonances

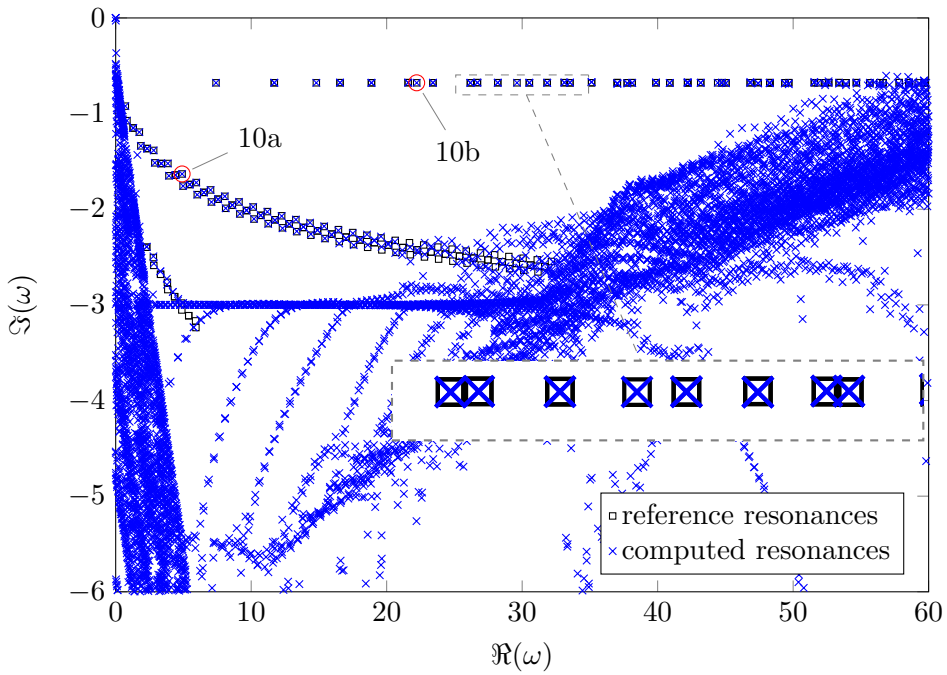

Figure 12: Computed resonances of a two dimensional resonance problem using classical complex scaling with $\sigma(\omega) := \frac{9+9i}{\omega}$). The reference resonances where calculated using higher polynomial order.

are the ones raising problems, especially since the location of the exterior spurious resonances delicately depends on the choice of the damping parameter.

Moreover, we have studied the use of a frequency dependent damping parameter resulting in a polynomial eigenvalue problem. In this case the same classes of spurious resonances appear, but take different shapes than in the frequency independent case: The exterior spurious resonances keep constant distance to the real axis, since the absolute value of the complex scaled resonance function no longer depends on the frequency in the exterior domain. Thus, resonances near the real axis are not polluted by exterior spurious resonances. Moreover, if the damping parameter is chosen within reasonable bounds it has no impact on the number of well approximated correct resonances.

If the solution of the non-linear eigenvalue problems should be avoided, the frequency depending scaling can still be used as a filter for the resonances computed with frequency independent scaling. Plugging the results of the linear eigenvalue problem into the discretization matrices of the frequency dependent scaling should lead to large condition numbers, if the result is the approximation of a resonance to the non-linear, frequency scaled resonance problem. So truncation and exterior spurious resonances can be detected by this procedure. Of course for this application a precise knowledge of the spectral properties of the non-linear eigenvalue problem resulting from frequency dependent complex scaling is crucial. So this paper might help to construct a reliable filter for spurious resonances as well.

References

[1] M. Abramowitz and I. A. Stegun, *Handbook of mathematical functions with formulas, graphs, and mathematical tables*, vol. 55 of National Bureau of Standards Applied Mathematics Series, For sale by the Superintendent of Documents, U.S. Government Printing Office, Washington, D.C., 1964.

[2] J.-P. Berenger, *A perfectly matched layer for the absorption of electromagnetic waves*, J. Comput. Phys., 114 (1994), pp. 185–200.

[3] A. Bermúdez, L. Hervella-Nieto, A. Prieto, and R. Rodríguez, *An exact bounded perfectly matched layer for time-harmonic scattering problems*, SIAM J. Sci. Comput., 30 (2007/08), pp. 312–338.

[4] W.-J. Beyn, *An integral method for solving nonlinear eigenvalue problems*, Linear Algebra Appl., 436 (2012), pp. 3839–3863.

[5] J. H. Bramble and J. E. Pasciak, *Analysis of a finite PML approximation for the three dimensional time-harmonic Maxwell and acoustic scattering problems*, Math. Comp., 76 (2007), pp. 597–614 (electronic).

[6] W. C. Chew and W. H. Weedon, *A 3d perfectly matched medium from modified Maxwell's equations with stretched coordinates*, Microwave Optical Tech. Letters, 7 (1994), pp. 590–604.

[7] F. Collino and P. Monk, *The perfectly matched layer in curvilinear coordinates*, SIAM J. Sci. Comput., 19 (1998), pp. 2061–2090 (electronic).

[8] D. Colton and R. Kress, *Inverse acoustic and electromagnetic scattering theory*, vol. 93 of Applied Mathematical Sciences, Springer-Verlag, Berlin, second ed., 1998.

[9] M. Halla, *Convergence of hardy space infinite elements for helmholtz scattering and resonance problems*, SIAM Journal on Numerical Analysis, 54 (2016), pp. 1385–1400.

[10] S. Hein, T. Hohage, W. Koch, and J. Schöberl, *Acoustic resonances in high lift configuration*, J. Fluid Mech., 582 (2007), pp. 179–202.

[11] P. D. Hislop and I. M. Sigal, *Introduction to spectral theory*, vol. 113 of Applied Mathematical Sciences, Springer-Verlag, New York, 1996. With applications to Schrödinger operators.

[12] T. Hohage and L. Nannen, *Hardy space infinite elements for scattering and resonance problems*, SIAM J. Numer. Anal., 47 (2009), pp. 972–996.

[13] ——, *Convergence of infinite element methods for scalar waveguide problems*, BIT Numerical Mathematics, 55 (2015), pp. 215–254.

[14] T. Hohage, F. Schmidt, and L. Zschiedrich, *Solving time-harmonic scattering problems based on the pole condition. II. Convergence of the PML method*, SIAM J. Math. Anal., 35 (2003), pp. 547–560.

[15] F. Ihlenburg, *Finite element analysis of acoustic scattering*, vol. 132 of Applied Mathematical Sciences, Springer-Verlag, New York, 1998.

[16] B. Kettner, *Detection of spurious modes in resonance mode computations*, PhD thesis, Free University Berlin, 2012.

[17] S. Kim and J. E. Pasciak, *The computation of resonances in open systems using a perfectly matched layer*, Math. Comp., 78 (2009), pp. 1375–1398.

[18] ——, *Analysis of the spectrum of a Cartesian perfectly matched layer (PML) approximation to acoustic scattering problems*, J. Math. Anal. Appl., 361 (2010), pp. 420–430.

[19] M. Lassas and E. Somersalo, *On the existence and the convergence of the solution of the pml equations*, Computing, 60 (1998), pp. 229–241.

[20] N. Moiseyev, *Quantum theory of resonances: Calculating energies, width and cross-sections by complex scaling*, Physics reports, 302 (1998), pp. 211–293.

[21] L. Nannen, *Hardy-Raum Methoden zur numerischen Lösung von Streu- und Resonanzproblemen auf unbeschränkten Gebieten*, PhD thesis, University of Göttingen, Der Andere Verlag, Tönning, 2008.

[22] S. A. Sauter and C. Schwab, *Boundary element methods*, vol. 39 of Springer Series in Computational Mathematics, Springer-Verlag, Berlin, 2011.

[23] F. Schenk, *Optimization of resonances for multilayer x-ray resonators*, PhD thesis, University of Göttingen, 2011. http://resolver.sub.uni-goettingen.de/purl?gs-1/7051.

[24] J. Schöberl, *Netgen - an advancing front 2d/3d-mesh generator based on abstract rules*, Comput.Visual.Sci, 1 (1997), pp. 41–52.

[25] ——, *C++11 implementation of finite elements in ngsolve*, Preprint 30/2014, Institute for Analysis and Scientific Computing, TU Wien, 2014.

[26] B. Simon, *The theory of resonances for dilation analytic potentials and the foundations of time dependent perturbation theory*, Ann. Math., 97 (1973), pp. 247–274.

[27] O. Steinbach and G. Unger, *Convergence analysis of a Galerkin boundary element method for the Dirichlet Laplacian eigenvalue problem*, SIAM J. Numer. Anal., 50 (2012), pp. 710–728.

[28] M. E. Taylor, *Partial differential equations. II*, vol. 116 of Applied Mathematical Sciences, Springer-Verlag, New York, 1996. Qualitative studies of linear equations.